IOP Conf. Series: Materials Science and Engineering **63** (2014) 012016 doi:10.1088/1757-899X/63/1/012016

Surface flow in severe plastic deformation of metals by sliding

A Mahato, Y Guo[1], H Yeung and S Chandrasekar

Center for Materials Processing and Tribology, Purdue University, West Lafayette, IN 47907
[1] M4 Sciences LLC, West Lafayette, IN 47906

E-mail: chandy@purdue.edu

Abstract. An *in situ* study of flow in severe plastic deformation (SPD) of surfaces by sliding is described. The model system - a hard wedge sliding against a metal surface - is representative of surface conditioning processes typical of manufacturing, and sliding wear. By combining high speed imaging and image analysis, important characteristics of unconstrained plastic flow inherent to this system are highlighted. These characteristics include development of large plastic strains on the surface and in the subsurface by laminar type flow, unusual fluid-like flow with vortex formation and surface folding, and defect and particle generation. Preferred conditions, as well as undesirable regimes, for surface SPD are demarcated. Implications for surface conditioning in manufacturing, modeling of surface deformation and wear are discussed.

1. Introduction

The use of sliding-type deformation to impose large plastic strains on surfaces is a central feature of many surface conditioning (deformation) processes for metals such as friction stir processing, burnishing, surface mechanical grinding, sliding, peening and even machining [1-3]. Intrinsic to this surface SPD is unconstrained plastic flow, which differs from the constrained flow more common to deformation processing. Unconstrained plastic flow by sliding-type deformation is also ubiquitous in wear of metal surfaces by abrasion, adhesion and delamination [4, 5]. In all of these instances, the surfaces show extensive deformation, as do the chips and particles generated by the processes. This is a consequence of high pressures, on the order of the material hardness, applied by an indenter (asperity, tool) sliding on the surface. A basic understanding of the characteristics of surface plastic flow should be of value in designing surface conditioning processes, and in analyzing and controlling wear at sliding metal interfaces [6].

The typical experimental approach that has been used in studying surface flow is investigation of the resultants of the process system at various stages and reconstructing a picture of what is going on [7]. The problem with this "post-mortem" examination is that evidence of the critical, unit material interaction events is often masked or erased. Nevertheless, this type of examination has led to important insights into flow phenomena occurring in surface conditioning and wear [5, 8]. It has also enabled analytical models of the processes to be formulated using continuum approaches - slip line field (SLF), shake-down and finite element analyses (FEA) [9, 10].

A complementary experimental approach to studying these flow phenomena is by *in situ* investigation of the process zone with a model sliding system, wherein the unit events relevant to surface conditioning processes and wear can be directly observed. Such a system is provided by the sliding contact between a sharp wedge (tool, asperity) and a surface under conditions of plane strain (2D) deformation [1, 9]. The present work describes an *in situ* study of material flow in metal surfaces

created by a hard wedge indenter. The observations pertain to material flow in the process zone, strain/strain rate fields, imposition of large plastic strains on the surface, and wear particle formation.

2. Experimental

The experimental system (Fig. 1) consisted of a workpiece (WP) in the form of a plate sliding against a hard steel wedge indenter at speeds V of up to 50 mm/sec [11, 12] under conditions of 2-D deformation. The relatively low speeds minimize temperature influences. A sharp indenter edge (< 10 µm edge radius) was used to minimize rubbing-induced deformation at the indenter-WP contact. The indenter rake angle (α) is adjusted by changing the orientation of the indenter and the depth of tool-work interaction (h_o) is varied by using a micro-stage (Fig. 1). The WP systems were commercially pure Al (grain size ~ 200 µm) and OFHC Cu (grain size ~ 118 µm) in an initial annealed condition. The flow of metal in the process zone was observed using a high-speed imaging system (PCO dimax CMOS camera) coupled to an optical microscope assembly (Nikon Optiphot). Flow patterns and quantitative details of the deformation were obtained by application of Particle Image Velocimetry (PIV) to the image sequences [11, 13]. PIV involves use of tracers or particles dispersed in the medium and tracking the motion of particle ensembles by digitizing high-speed images of the 'flow' [14, 15]. The particles in the experiments were 'asperities' - roughness features deliberately introduced onto the WP surface being imaged by abrasion with 1200 grit SiC paper. An optically transparent glass plate was used to lightly constrain the imaged side so as to minimize out-of-plane flow of material during the sliding. The camera sensor had a full resolution of 2016 x 2016 pixel and physical size of 22.18 x 22.18 mm. Images could be recorded at up to 1279 fps using the full sensor area. Higher imaging speeds could be achieved by reducing the sensor area; for example, when the image size is 1296 x 720 pixel, framing rates of up to ~5000 fps are possible. The PIV analysis was used to estimate displacement/velocity and strain/strain rate fields in the deformation zone [11, 13, 16], and characterize the SPD. Stream-, streak- and path- lines of flow (analogous to fluid flow) were obtained from the displacement and velocity fields [12]; these were particularly useful for visualizing the flow features.

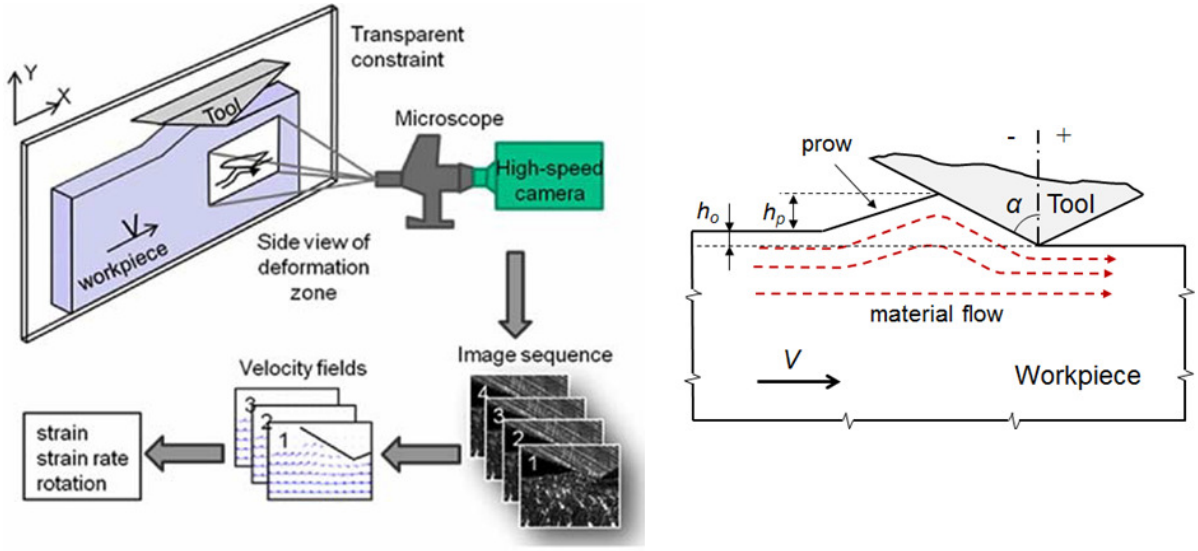

Figure 1. Schematic of the experimental setup (left) and parameters (right).

3. Results

The *in situ* imaging and the PIV analysis have revealed interesting, including hitherto little known, aspects of unconstrained plastic flow and SPD in sliding contact.

Flow patterns Figure 2a shows one frame from a high speed image sequence of lubricated sliding of Al with α = -75°. A prow of material of height h_p is seen to build up ahead of the wedge, similar to that noted and analyzed in prior sliding experiments [17]. The superimposed streaklines derived from the high speed images indicate a smooth steady flow analogous to laminar (fluid) flow. This flow pattern is similar to that usually assumed in SLF analysis of sliding. The effective strain rate ($d\varepsilon/dt$) field for this sliding condition is shown in Fig. 2b, while Fig. 2c shows the strain rate variation along 3 particle paths. Two regions of intense strain rate – one in the prow region (A) and the other in the vicinity of the indenter tip (B) – may be noted (Fig. 2b). The maximum $d\varepsilon/dt$ is ~ 12/s and occurs in the indenter tip region B. Other PIV measurements showed $d\varepsilon/dt$ to increase approximately linearly with V.

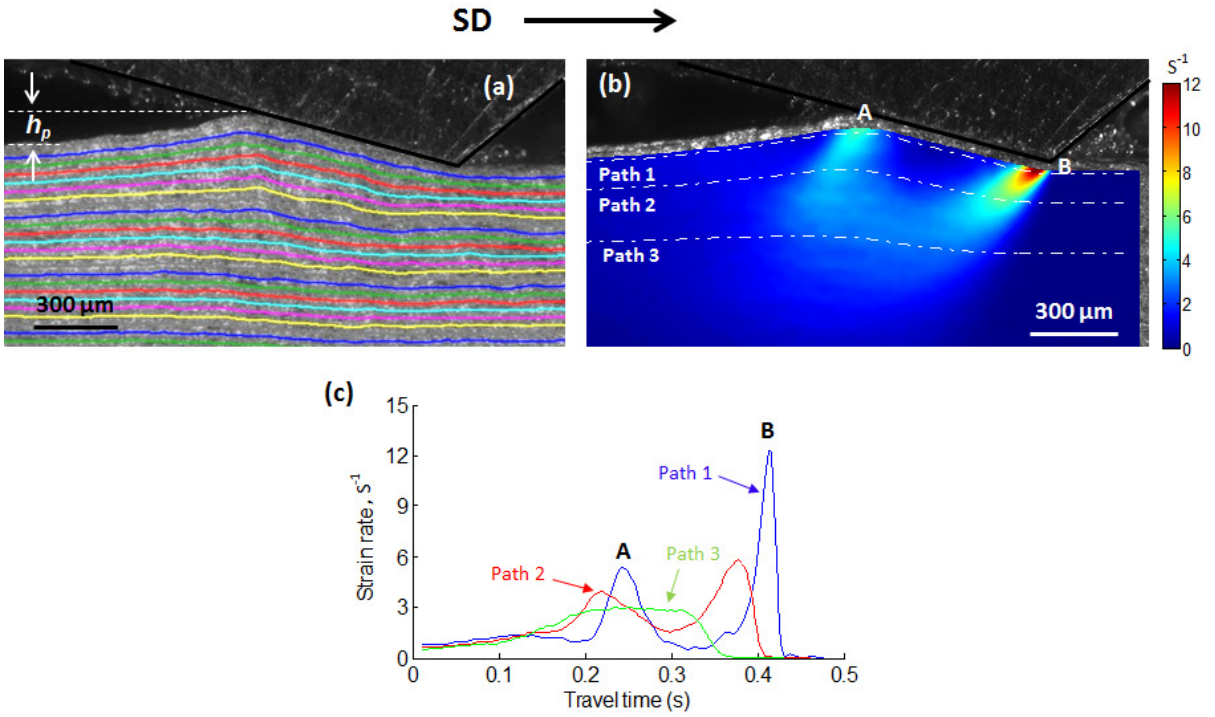

Figure 2. Prow formation and laminar flow in sliding of Al: (a) image with superimposed streak lines showing laminar type of flow, (b) strain rate field after 1 pass of sliding, and (c) time histories of strain rate for material points travelling along the pathlines shown in (b). α = –75°, V = 5mm/s, 1000 fps, fluid: Mobil 1. SD - sliding direction of WP.

The strain (ε) field is obtained by accumulating the incremental strain – that is integration of the $d\varepsilon/dt$ field - along particle paths such as 1-3; this field is plotted in Fig. 3. This laminar strain field is seen to be quite homogeneous with a surface ε value of ~ 1. Also, this strain is uniformly distributed to a depth of ~ 250 µm into the subsurface. The depth of the uniformly strained region was found to scale with h_p; h_p in turn is determined by h_0 and the ductility of the surface layer. It is of interest to note here that the corresponding large strain field imposed by material removal processes such as machining not only extends to a much smaller depth (~ 20 µm) but is also much less uniformly distributed into the subsurface [11], compared to this sliding field.

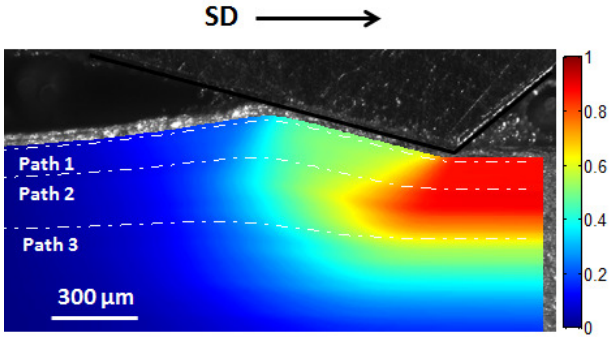

Figure 3. Subsurface strain field (averaged) in the Al after 1 sliding pass. The path lines of Fig. 2b are superimposed onto the strain field. α = –75°, V = 5 mm/s, 1000 fps, fluid: Mobil 1. SD - sliding direction of WP.

The characteristics of the laminar flow pattern and strain field in OFHC Cu were found to be similar to that in the Al. Figure 4 shows the variation of ε with depth into the subsurface for Cu in multiple pass sliding, as measured by the PIV. The ε imposed in each of the 1st, 2nd and 4th passes of sliding is given in Fig. 4a. It is clear from these measurements that a uniformly strained region of depth ~ 400 µm is created by each pass of sliding, be it the first or a subsequent pass. The ε per pass (~ 0.8 - 1.6) is, however, influenced by the prior deformation of the surface. The total ε accumulated in the 4 sliding passes and its variation with depth is shown in Fig. 4b. A uniformly strained layer, with ε ~ 5 and of depth ~ 400 µm, is seen to be created on the surface. Below this depth, the ε value decreases somewhat steeply; the overall depth of the strained layer (uniform + non-uniform region) is ~ 800 µm. Strains as large as 12 have been measured on the surface after 8-10 passes in this sliding mode. These measurements show that a laminar-type surface flow mode coupled with multiple-pass sliding is quite suitable, perhaps ideal, for imposing large uniform strains over substantial depths on metal surfaces.

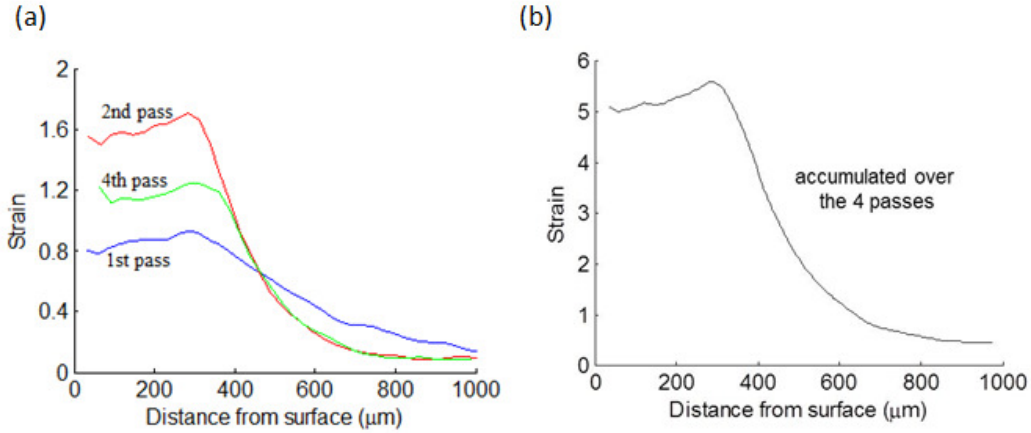

Figure 4. Subsurface strain in multiple pass sliding of OFHC Cu under laminar flow conditions: a) strain accumulated in each pass, and b) total strain accumulated in the 4 sliding passes. α = -70°, V = 1mm/s, h_0 = 100 µm, fluid: Coolube 2210.

SLF and other continuum analyses of sliding predict that the surface ε value should increase when α is made less negative, enabling greater levels of ε to be imposed in a sliding pass [1, 17]. As this would be beneficial for surface SPD processing (e.g., microstructure refinement), in that larger strains could be imposed in fewer passes, a study was made of the effect of α on ε. Figure 5 shows a typical measured strain field in sliding of Al for α = -65°. The surface ε levels (~ 2 - 2.5) are indeed much

greater than for α = -75° (Fig. 3). But considerable variation is seen in the strain values on the residual surface in the wake of the wedge, along with steeper strain gradients into the subsurface. The surface strain pattern shows a "lamellar" structure along the WP length with alternating regions of higher and lower ε. This is certainly undesirable from an SPD processing standpoint and is, certainly, contrary to SLF predictions.

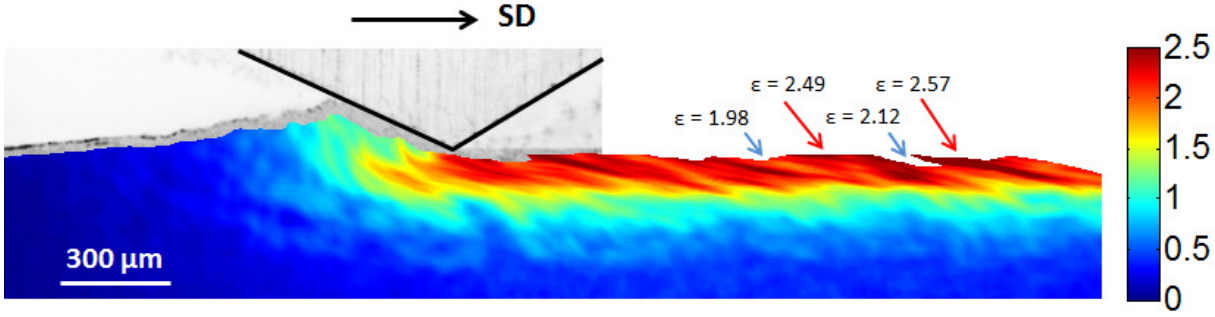

Figure 5. Subsurface strain field in the Al after 1 sliding pass for α = -65°. The red arrows show regions of strain concentration on the surface while the blue arrows point to the less strained regions. V = 5 mm/s, 1000 fps, fluid: Mobil 1. SD – sliding direction of WP.

Examination of flow patterns from high speed image sequences have provided the answer to the origin of the strain heterogeneity observed at the less negative rake angles. Furthermore, they have revealed an unusual, non-steady surface flow (Fig. 6) – with highly sinuous near-surface streakline pattern - that until recently appears to have not been highlighted [12]. Figures 6a-d show the evolving flow pattern using 4 frames from a high speed image sequence for α = -65°. The outstanding features of this pattern are the formation of small "bumps" - surface protuberances – ahead of the wedge, and the occurrence of self-contacts between successive bumps that result in fold-like features (folds) on the surface. The green and red arrows in Fig. 6a show the position of two bumps ahead of the wedge. With continued sliding, these bumps grow in height to ~ 50-100 µm while coming closer together and interacting to make a self-contact (fold); one such fold can be seen at white arrow in Fig. 6b. The propagation and evolution of this fold – a surface instability - is shown in Figs. 6c and d. Fold formation precedes contact with the wedge face. Multiple folds may be seen traversing the wedge-WP contact face in Figs. 6c and d. The development of these folds is also well revealed in the changes in the curvature of the streak lines immediately below the "surface". As a fold exits the contact, its orientation is changed by stretching and rotation. Crack- and tear- like features are left behind on the surface – defect remnants of the folds - in the wake of the wedge, see for example at white arrow in Fig. 6d. The sinuous nature of the streak lines at this sliding condition, and the fold patterns, indicate that the flow is highly non-laminar and vortex-like at this sliding condition, in contrast to Fig. 2. This flow is quite different from that commonly assumed (or predicted) in triboplasticity [9, 10]. Bumps and folds were found to become more frequent at smaller negative rake angles.

Heterogeneous plastic flow arising from the grain structure in polycrystalline metals has been identified as the cause for the bump-formation (via local variations in deformation) and ensuing folding observed under the non-laminar flow conditions [12]. The key parameters influencing folding were found to be the ratio of the grain size to prow height (h_p), ductility of the surface layer and interface friction.

The non-uniformity in the surface strain distribution in Fig. 5 is a consequence of the non-laminar surface flow and surface folding, with each strain lamella corresponding to the residue from a fold. The peak strain value on the residual WP surface associated with a fold is ~ 2.5 (Fig. 5), substantially higher than that noted for the laminar flow strain field and also ~ 25 percent greater than that occurring in the non-folded areas of the surface.

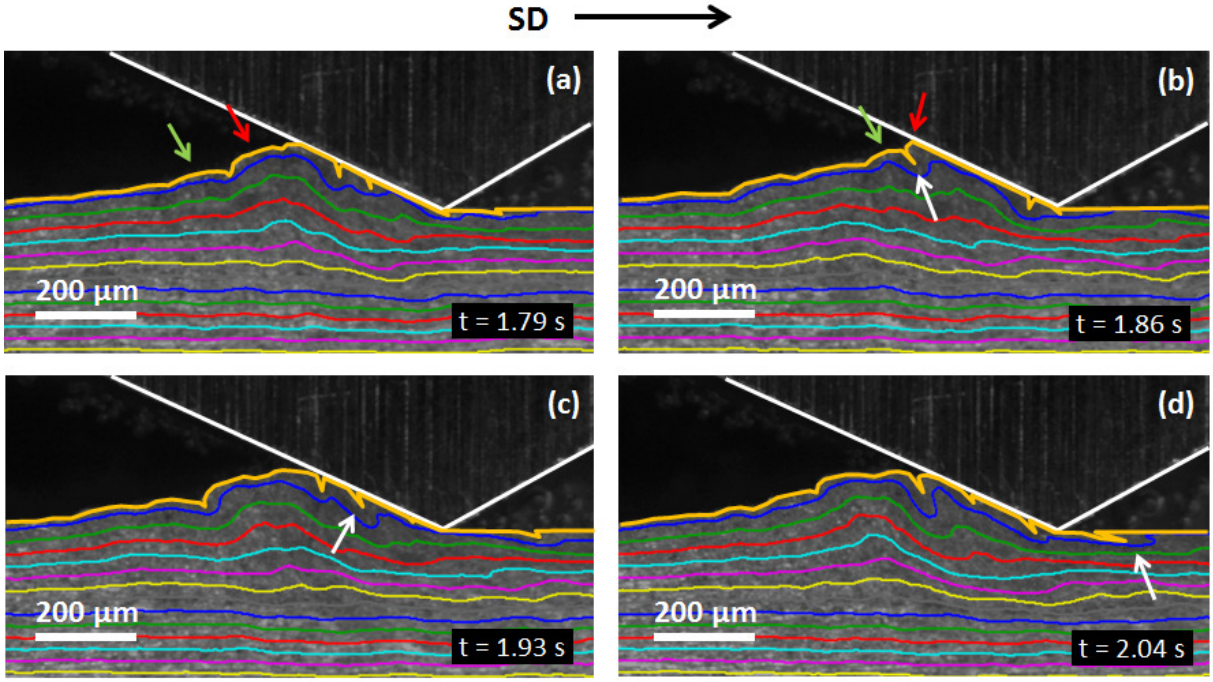

Figure 6. Four frames with streak-lines from a high speed image sequence showing development of bumps and folds in Al. α = -65°, V = 5 mm/s, fluid: Mobil 1, 1000 fps. The green and red arrows show evolution of specific bumps, while the white arrow shows evolution of a specific fold into a crack-like feature on the residual surface. SD - sliding direction of WP.

Wear particles When a fold (red arrow in Fig. 7a) emerges from the contact region, it splits leaving behind a tear (blue arrow in Fig. 7b) and a complementary crack-like feature (green arrow in Fig. 7b) on the surface. Figures 7c and d show SEM pictures of the crack-like features and tears on the surface. The tears usually project upward and in a direction opposite to that of the crack-like features. Since these latter features are usually embedded in the subsurface, they may not be visible in a surface examination. Metallographic examination of the subsurface, however, is adequate to reveal them. In a subsequent sliding pass of the wedge, the tear- and crack- like features are "dislodged" from the surface resulting in wear particles. This is a barrier to surface SPD by the application of repeated sliding passes at this α.

The folds and tears resemble closely, features seen on surfaces after sliding wear [5, 18], delamination [19] and abrasion [20]. However, past studies have attributed the occurrence of these features to origins other than fold formation. Folding, tears and crack-like features have also been observed in sliding of copper and brass [12]. The present observations also show that wear particles can develop in sliding by a folding-type mechanism in as little as 1-2 sliding passes. It suggests a mechanism for moderate/severe sliding wear that does not require chip formation by cutting due to asperities interacting with a surface, as postulated by Kopalinsky and Oxley [10] and Johnson [9]. In fact, formation of wear particles by cutting requires asperity incidence angles much greater than those typical of sliding contacts.

The observations of the present study should hold equally well for other tool and WP geometries (e.g., cylinder, sphere), if the local rake angle is used in place of the wedge rake angle.

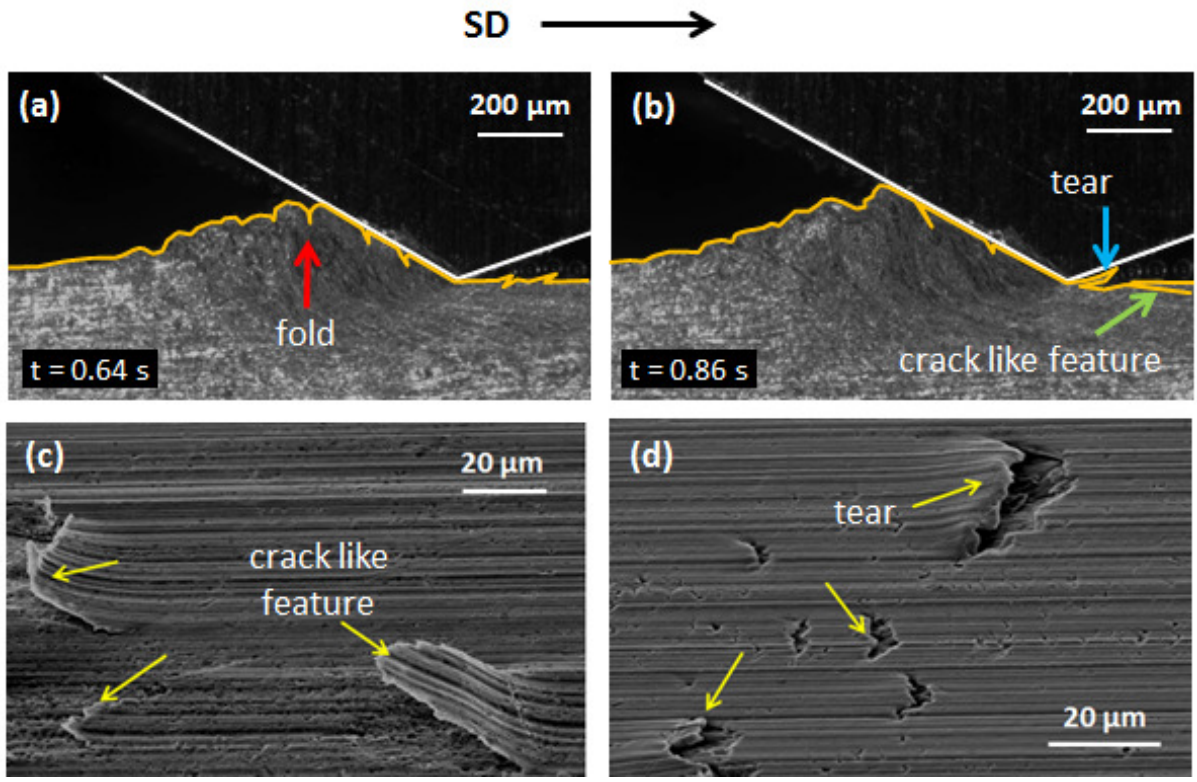

Figure 7. Two frames from a high speed image sequence showing formation of tear- and crack-like features on the Al surface. The blue and green arrows point to a tear and a (complementary) crack-like feature, respectively, formed by splitting of the fold shown in a) as it exits the contact. SEM micrographs showing typical (c) crack-like features and (d) tears on the Al surface in the wedge wake. $\alpha = -60°$, V = 5 mm/s, 1000 fps, fluid: Mobil 1. SD – sliding direction of WP.

4. Summary and Implications

The high-resolution, *in situ* study of deformation produced by a sliding wedge has revealed unique aspects of unconstrained plastic flow at metal surfaces. At very large negative rake angles, a smooth laminar flow pattern prevails under the wedge. The corresponding flow field is characterized by uniform strains of ~ 1 (per sliding pass) extending to large depths into the subsurface. At this sliding condition, the strained layer on the surface can be accumulated to large levels, using multiple sliding passes, making it the preferred configuration for surface SPD processing. This type of laminar-SPD processing can be implemented for surface conditioning of curved surfaces as well using commonly available equipment. A highly non-laminar type of flow takes over when the wedge rake angle is made less negative. This type of flow triggers formation of primitive vortex-like structures and folds on the surface; and tears and crack-like features in the wake of the wedge due to the folding. Since the surface strain now is quite non-homogeneous, and, furthermore, the tears and cracks can produce wear particles by delamination in as few as 1-2 sliding passes, multiple pass SPD becomes infeasible at this condition. The non-laminar flow is not predicted by the common continuum approaches used to model surface deformation processes and triboplasticity.

Some implications of the study for surface conditioning and sliding wear may be noted: the need to utilize deformation geometries (local rake angles) that promote laminar-type flow for multi-pass surface SPD; control of grain size of the initial workpiece material for improved surface conditioning and reducing sliding wear; consideration of folding as an important mechanism for formation of wear particles, and re-assessment of current mechanisms for wear particle generation in sliding and abrasive

machining systems; and incorporating material surface heterogeneity in modeling of surface deformation processing and triboplasticity.

Future work will explore the effects of variables such as material grain size, ductility and temperature (high speed sliding) on the flow phenomena.

5. Acknowledgements

The research was supported in part by US Army Research Office grant W911NF-12-1-0012, and NSF grants CMMI 1234961 and IIP 1237866. We are grateful to Dr. Suveen Mathaudhu of the U.S. Army Research Office for discussions and encouragement. We would like to thank Dr. Dinakar Sagapuram for help with some of the SEM work.

References

[1] Oxley P L B 1989 *The mechanics of machining: an analytical approach to assessing machinability* (New York, Halsted Press)
[2] Zhu K Y, Vassel A, Brisset F, Lu K, and Lu J 2004 *Acta Mater.* **52** pp 4101-4110
[3] Hughes D A, and Hansen N 2001 *Phys. Rev. Lett.* **87** 135503
[4] Hutchings I M 2003 *Tribology: friction and wear of engineering materials* (Oxford, Butterworth Heinemann)
[5] Samuels L E, Doyle E D and Turley D M 1981 *Fundamentals of friction and wear of materials* ed D A Rigney (Materials Park, Ohio: American Society for Metals) pp 13-41
[6] Whitehouse D J 1978 *Fundamentals of Tribology*: *Proceedings of the International Conference on the Fundamentals of Tribology* ed N P Suh et al (Cambridge: MIT Press) pp 17-52
[7] Tabor D 1977 *Wear of Materials* ed Glaeser et al (New York: The American Society of Mechanical Engineers) pp 1-11
[8] Scott D, Seifert W W and Westcott V C 1974 *Sci. Am.* **230** pp 88-97
[9] Johnson K L 1995 *Wear* **190** pp 162-170
[10] Kopalinsky E M and Oxley P L B 1995 *Wear* **190** pp 145-154
[11] Guo Y, Saldana C, Compton W D and Chandrasekar S 2011 *Acta Mater.* **59** pp 4538-4547
[12] Sundaram N K, Guo Y and Chandrasekar S 2012 *Phys. Rev. Lett.* **109** 106001
[13] Gnanamanickam E P, Lee S, Sullivan J P and Chandrasekar S 2009 *Meas. Sci. Technol.* **20** 095710
[14] Adrian R J 1991 *Annu. Rev. Fluid Mech.* **23** pp 261-304
[15] Raffel M, Willert C E, Wereley S T and Kompenhans J 2007 *Particle image velocimetry: a practical guide* (Berlin, Springer Verlag)
[16] Brown T L, Saldana C, Murthy T G, Mann J B, Compton W D, Trumble K P, King A H and Chandrasekar S 2009 *Acta Mater.* **57** pp 5491-5500
[17] Rowe G W and Wetton A G 1965 *Wear* **8** pp 448-454
[18] Rigney D A 1988 *Annu. Rev. Mater. Sci.* **18** pp 141-163
[19] Jahanmir S and Suh N P 1977 *Wear* **44** pp 17-38
[20] Malkin S 1989 *Grinding technology: theory and applications of machining with abrasives* (New York, Halsted Press)